

# Photosensitization of Thin SnO<sub>2</sub> Nanocrystalline Semiconductor Film Electrodes with Metalloporphyrin

Fernando Fungo, Luis Otero, Edgardo N. Durantini, Juana. J. Silber, and Leonides E. Sereno\*

Departamento de Química y Física, Universidad Nacional de Río Cuarto, Agencia Postal 3, 5800 Río Cuarto, Argentina

Received: January 11, 2000; In Final Form: March 23, 2000

Sensitized photocurrent generation is observed with a porphyrin dyad (**P<sub>Zn</sub>-P**) and its structural moieties: 5-(4-carboxyphenyl)-10,15,20-tris(4-methylphenyl) porphyrin (**P**) and Zn(II) 5-(4-carboxyphenyl)-10,15,20-tris(4-methylphenyl) porphyrin (**P<sub>Zn</sub>**). The dyes were adsorbed to saturation on a nanocrystalline SnO<sub>2</sub> thin film, employed as working electrode in a photoelectrochemical cell. The metallized and unmetallized moieties possess different singlet state energies and redox properties. In both, solution and adsorbed state, nearly complete singlet–singlet energy transfer from the **P<sub>Zn</sub>** to **P** has been determined in the dyad. **P<sub>Zn</sub>** is less efficient than **P** in the photocurrent generation, but is a suitable energy donor in the dyad molecule. The generation of photoelectrical effects by the dyad is less effective in comparison with **P**. Considering the oxidation potentials of the two moieties in **P<sub>Zn</sub>-P**, a mechanism is proposed where the oxidized metallized porphyrin enhances the back electron-transfer process.

## 1. Introduction

Photoinitiated transmembrane electron transfer to yield long-lived charge-separated states is the basic energy conversion process of natural photosynthesis. In the protein environment of photosynthetic reaction centers it is carried out by a series of short-range, fast, and efficient electron-transfer steps, which move electrons and holes to opposite sides of the membrane. The actual photochemistry involves chlorophyll derivatives, quinones, and carotenes. Photoinduced electron-transfer involving cyclic tetrapyrrole molecules (the special pair of bacteriochlorophylls) is the primary step in the mechanism of photosynthetic bacteria, where singlet–singlet energy transfer between tetrapyrroles is also important.<sup>1</sup> Given the crucial role of photosynthesis in natural solar energy conversion, it is not surprising that great effort has been made to mimic this solar energy harvesting device.<sup>2,3</sup>

Synthetic multicomponent molecules that mimic both energy and electron transfer have been reported<sup>4</sup> and, in a recent work, Gust et al. reported an artificial photosynthetic membrane.<sup>5</sup> In this membrane a vectorial photoinduced electron transfer is produced in a carotene–porphyrin–naphthoquinone (C–P–Q) molecular triad, which generates a proton pump. The photogenerated C<sup>•+</sup>–P–Q<sup>•-</sup> state is coupled to proton translocation by quinones that alternate between reduced and oxidized forms.<sup>5</sup>

Like the photosynthetic reaction center, many artificial photosynthetic assemblies incorporate metalloporphyrins because they can be reversibly reduced and oxidized.<sup>6,7</sup> Chlorophyll derivatives and several related porphyrins have been used as light receptors in energy conversion devices,<sup>8–23</sup> often in achieving spectral sensitization of wide band gap semiconductors.<sup>10–19</sup>

The energy difference between the conduction band edge of an *n*-type semiconductor film and the oxidation potential of the excited sensitizer ( $E_{ox}^*$ ) present as an adsorbate provides a

driving force for excited-state charge injection.<sup>24,25</sup> Unfortunately, however, only the first monolayer of the adsorbed dye produces a significant photoeffect, and the light-harvesting efficiency of a single monolayer is very low. Nevertheless, in a porous film of nanometer-sized semiconductor particles, the effective surface area can be greatly enhanced, producing substantial light absorption even with only a monolayer of dye on each particle.<sup>26–35</sup> As it has been pointed out,<sup>10,11,29</sup> there are several analogies between the natural photosynthesis and the dye-sensitized nanocrystalline semiconductor electrodes. Nature uses a similar method of absorption enhancement by stacking the chlorophyll-containing thylakoid membranes of the chloroplast to form the grana structure.<sup>10</sup>

Spectral sensitization of porous metal oxides by adsorbed chlorophylls and related porphyrins has been studied using ZnO,<sup>12</sup> SnO<sub>2</sub>,<sup>13,14</sup> and TiO<sub>2</sub>.<sup>10,11</sup> Light harvesting and charge separation efficiencies in a range of porphyrin dyes adsorbed on nanostructured TiO<sub>2</sub> were found comparable to those in natural photosynthesis, with a very high (nearly 80%) incident-photon-to-current efficiency (IPCE).<sup>10,11</sup> Similarly, Kamat et al. reported 15% efficiency for electron injection from adsorbed chlorophyll a and b into SnO<sub>2</sub>.<sup>13,14</sup> With such high efficiencies, the photosensitization of oxide semiconductors has become a practical means for solar energy conversion. Using Ru(II) bipyridine complexes as photosensitizers, net power conversion efficiencies up to 10% have been reported in diffuse daylight on nanoporous TiO<sub>2</sub> electrodes.<sup>26,36,37</sup>

In this study we have focused on a porphyrin dyad and its structural components (Figure 1), as photosensitizing adsorbates on nanocrystalline SnO<sub>2</sub> films, to extend the photoresponse of this large band gap semiconductor. Porphyrin dyad containing structural moieties with both different singlet state energies and redox properties can undergo singlet–singlet energy transfer or photoinduced electron transfer.<sup>38–43</sup> Then, it is possible that an “antenna” effect<sup>44</sup> is present in the spectral sensitization of a wide band-gap semiconductor. The use of a conventional semiconductor electrode and a simple molecular sensitizer light

\* To whom correspondence should be addressed. E-mail: sereno@arnet.com.ar

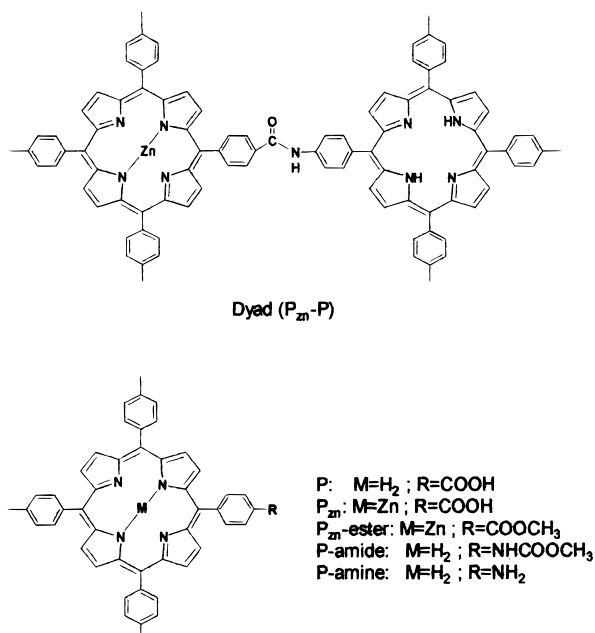


**Figure 1.** Structures of the sensitizing dyes.

absorption is often inefficient at monolayer coverage. One possibility to improve the overall efficiency is the use of some type of “antenna-sensitizer” molecular device. In principle, this device would use intercomponent energy transfer from an “antenna” chromophoric unit to a specific chromophoric unit that behaves at the same time as an energy collector and as a charge injection sensitizer.

## 2. Experimental Section

**Synthesis of Porphyrine Dyes.** The structure of the porphyrins used are shown in Figure 1. They were prepared using the dipyrromethane method.<sup>45–47</sup> The syntheses of 5-(4-carboxymethoxyphenyl)-10,15,20-tris(4-methylphenyl) porphyrin (**P-ester**), 5-(4-carboxyphenyl)-10,15,20-tris(4-methylphenyl) porphyrin (**P**), Zn(II) 5-(4-carboxyphenyl)-10,15,20-tris(4-methylphenyl) porphyrin (**P<sub>Zn</sub>**), and 5-(4-acetamidophenyl)-10,15,20-tris(4-methylphenyl) porphyrin (**P-amide**) have been previously reported.<sup>46–50</sup> **P-ester** was prepared by the reaction of 4-methylbenzaldehyde, 4-carboxymethylbenzaldehyde, and *meso*-(*p*-tolyl) dipyrromethane in CHCl<sub>3</sub>. The mixture was catalyzed by BF<sub>3</sub>·O(Et)<sub>2</sub> at room temperature. The chlorine compounds were oxidized to the corresponding porphyrins with 2,3-dichloro-5,6-dicyano-1,4-benzoquinone (DDQ). **P-ester** was purified by flash chromatography and basic hydrolysis of the **P-ester** afforded the desired **P** compound.<sup>47</sup>

**P<sub>Zn</sub>** was formed by the reaction between **P** and Zn(II) acetate in methanol/dichloromethane. Flash chromatography yielded the pure **P<sub>Zn</sub>**.<sup>47</sup>

**P-amide** was prepared as described above for **P**, using 4-methylbenzaldehyde, 4-acetamidobenzaldehyde, and *meso*-(*p*-tolyl)dipyrromethane. Flash column chromatography afforded the amide porphyrin, which was hydrolyzed in basic medium to yield 5-(4-aminophenyl)-10,15,20-tris(4-methylphenyl) porphyrin (**P-amine**).<sup>47</sup>

**P<sub>Zn</sub>-P** dyad was synthesized from the acid chloride derivative of **P<sub>Zn</sub>** and **P-amine** in a mixture of toluene and pyridine at room temperature. Flash column chromatography afforded the pure dyad.

Spectroscopic data of the porphyrin derivatives coincide with those previously reported.<sup>47</sup>

**Preparation of SnO<sub>2</sub> Nanocrystalline Films.** Optically transparent electrodes were cut from indium tin oxide (ITO) coated glass plates (1.3 mm thickness, 100 Ω/square) obtained from Delta Technologies. The ITO slides were cleaned in hot acetone in a Soxhlet apparatus and then rinsed several times, first in 2-propanol and then in pure water (obtained from Labonco equipment model 90901-01) in an ultrasound bath. An SnO<sub>2</sub> colloidal suspension (particle diameter 20–30 Å, Alfa Chemicals) was used without further purification. A 1.5% SnO<sub>2</sub> suspension was prepared by dilution of the commercial compound with water containing a surfactant (0.01% Triton X-100, Aldrich), and the pH was adjusted to 10 using NH<sub>4</sub>OH. ITO/SnO<sub>2</sub> electrodes were prepared by coating using Kamat’s procedure.<sup>32</sup> An aliquot of 0.1 mL of the diluted suspension was spread onto a clean ITO surface with a 3.5 cm<sup>2</sup> area, followed by drying of the electrodes over a warm plate (5 min at ~90 °C). Finally, the SnO<sub>2</sub> films were annealed at 450 °C for 1 h. The resulting films, which are transparent in the visible region, have strong absorption in the UV with an onset at around 355 nm. (This onset absorption corresponds to a bulk band gap of 3.5 eV.)

The ITO/SnO<sub>2</sub> electrodes were modified with **P**, **P<sub>Zn</sub>**, and dyad **P<sub>Zn</sub>-P** porphyrins (Figure 1) by soaking the ITO/SnO<sub>2</sub> films in a saturated petroleum ether solution of the dye for a period of 2 h. The electrode was then washed with the same solvent, dried in a nitrogen stream and stored in vials. The violet–green coloration of the film confirms the adsorption of the dyes. These electrodes will be referred to as ITO/SnO<sub>2</sub>/dye or specifically ITO/SnO<sub>2</sub>/**P**; ITO/SnO<sub>2</sub>/**P<sub>Zn</sub>**, and ITO/SnO<sub>2</sub>/**P<sub>Zn</sub>-P** for modification with **P**, **P<sub>Zn</sub>**, or dyad **P<sub>Zn</sub>-P**, respectively. A copper wire was connected to the electrode surface with an indium solder.

**Absorption and Emission Spectroscopy.** Absorption spectra were measured with Shimadzu 2020 spectrophotometer. The fluorescence spectra of porphyrins in dichloromethane (DCM) solution and on ITO/SnO<sub>2</sub> electrodes were collected on a SPEX Fluoromax instrument.

**Electrochemistry.** For cyclic voltammetry (CV), a potentiostat–galvanostat EG & G Princeton Applied Research PAR-273 and a conventional three-compartment Pyrex cell were used. The working electrode was a Pt disk of 0.25 cm<sup>2</sup>. CV studies were carried out in 1,2-dichloroethane (DCE, Merck) containing 0.1 M tetrabutylammonium hexafluorophosphate (TBAHFP, Aldrich) as the supporting electrolyte. All of the potentials were referred to a saturated calomel electrode (SCE) and were corrected for IR drop by a positive feedback technique. Redox potentials for the first anodic and cathodic charge transfers of each molecule were calculated using the expression ( $E_p$  forward –  $E_p$  backward)/2.

**Photoelectrochemical Measurements.** Photoelectrochemical experiments were conducted in aqueous solutions (0.01 M) of hydroquinone (H<sub>2</sub>Q, Aldrich, recrystallized from toluene), with phosphate buffer (pH = 5.2) prepared from 0.05 M NaH<sub>2</sub>PO<sub>4</sub> (Anedra > 99%) and NaOH (Baker).<sup>17</sup> These solutions were degassed by bubbling with Ar and maintained in the top of the cell by continuous stream.

The measurements were carried out in a 10 mm quartz photoelectrochemical cell equipped with Ag/AgCl as the reference electrode and Pt foil as the auxiliary electrode. A battery-operated, low-noise potentiostat, constructed in our laboratory, was used in all photoelectrochemical measurements. The output signal of the photocurrent was recorded on a Radiometer-Copenaghe X-t recorder and the same recorder was used for measuring the generated photopotentials. Action spectra for ITO/SnO<sub>2</sub>/dye electrodes were obtained by sending the output of a

150 W high-pressure Xe lamp (Photon Technology Instrument, PTI) through a PTI high-intensity grating monochromator ( $\Delta\lambda = 5$  nm) and recording the resulting steady-state photocurrent. The electrodes were located at the focus of monochromator output (illuminated area:  $1\text{ cm}^2$ ). All of the photoelectrochemical measurements were done in front face configuration. The incident light intensities at different wavelengths were measured with a Coherent Laser-Mate Q radiometer (sensitivity  $1\ \mu\text{W}$ ).

### 3. Results and Discussion

**Photochemistry and Electrochemistry in Solution.** The dyad  $\mathbf{P}-\mathbf{P}_{\text{Zn}}$  contains structural moieties with both different singlet state energies and redox properties. Therefore, it is possible that an intramolecular singlet-singlet energy transfer or photoinduced electron transfer can occur after excitation. These events can also be present when the dyad is in adsorbed state, acting as spectral sensitizer of a wide band gap semiconductor. To assess these effects, the photochemistry and the electrochemistry of the three molecules were studied.

Investigation of the photochemistry of the monomers and dyad molecules was done by steady-state absorption and emission spectroscopy. The two porphyrin moieties in the dyad molecule are closely related, except that the central hydrogen atoms in the porphyrin bearing the acid group have been replaced by zinc. The absorption spectra of these compounds are shown in Figure 2. As can be observed, the spectrum of the dyad (Figure 2c) features four Q-band maxima at 515, 551, 592, and 648 nm, whereas the Soret band appears as a single maximum at 418 nm. Consequently, the absorption spectrum is identical to a linear combination of the spectra of the component chromophores (Figure 2a, b), within experimental error.<sup>38,46,47,51</sup> Thus, linkage of the chromophores does not lead to any significant changes in absorption band wavelengths, widths, or relative extinction coefficients.

On the other hand, in the emission spectra the situation changes. Figure 3 shows the corrected fluorescence spectra of the monomers units and the dyad in DCM solution. The  $\mathbf{P}_{\text{Zn}}$  has maxima at 598 and 646 nm, whereas  $\mathbf{P}$  has two maxima at 652 and 717 nm. The emission spectra of the dyad  $\mathbf{P}_{\text{Zn}}-\mathbf{P}$  resemble that of the unmetallized porphyrin, with no significant emission from the  $\mathbf{P}_{\text{Zn}}$  moiety, even though both porphyrin species absorb at the excitation wavelength (550 nm). These results suggest efficient and rapid singlet-singlet energy transfer from  $\mathbf{P}_{\text{Zn}}$  to the free base.<sup>38,42</sup>

Analyzing the possible photophysical mechanisms, the energies of the porphyrins' first excited singlet states can be calculated from the average of the frequencies of the longest wavelength absorption maxima and the shortest wavelength emission maxima. There is a significant energy gap between the  $\mathbf{P}_{\text{Zn}}$  first excited singlet state at 2.09 eV and that of  $\mathbf{P}$  at 1.9 eV. This means that the singlet energy transfer from the zinc porphyrin to the free base is an energetically favorable process.

On the other hand, it has been reported<sup>51</sup> that the reduction and oxidation potentials of the dimeric porphyrins are similar to those of the combined individual monomeric units, hence the energy of the charge separated state in  $\mathbf{P}_{\text{Zn}}^{+\bullet}-\mathbf{P}^{\bullet-}$  has been estimated from the first oxidation potential of  $\mathbf{P}_{\text{Zn}}-\text{ester}$  and the first reduction potential of  $\mathbf{P}-\text{amide}$  (Table 1) as determined from CV measurements. Typical results for  $\mathbf{P}-\text{amide}$  are shown in Figure 4.

As shown in Scheme 1, the  $\mathbf{P}_{\text{Zn}}^{+\bullet}-\mathbf{P}^{\bullet-}$  state lies at about 0.10 eV below  $\mathbf{P}_{\text{Zn}}$  first excited singlet state ( $^1\mathbf{P}_{\text{Zn}}-\mathbf{P}$ ). However, fluorescence excitation experiments reveal that singlet-singlet energy transfer from  $\mathbf{P}_{\text{Zn}}$  to the  $\mathbf{P}$  moiety is essentially quantita-

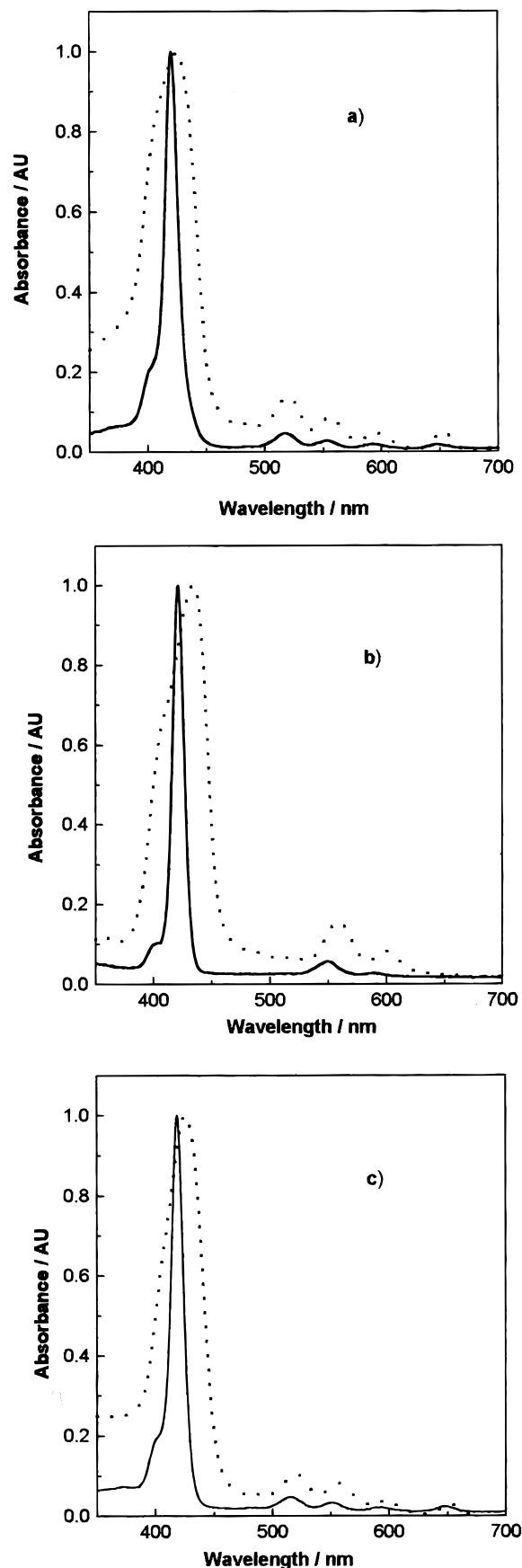


**Figure 2.** Absorption spectra of porphyrins: in solution of DCM (—) and in adsorbed state over ITO/SnO<sub>2</sub>/electrodes (- - -). (a)  $\mathbf{P}$ ; (b)  $\mathbf{P}_{\text{Zn}}$ , and (c)  $\mathbf{P}_{\text{Zn}}-\mathbf{P}$  dyad. Absorbances have been normalized to one.

tive (Figure 5). When fluorescence is monitored at 717 nm (where only  $\mathbf{P}$  emits), it can be seen that absorption and

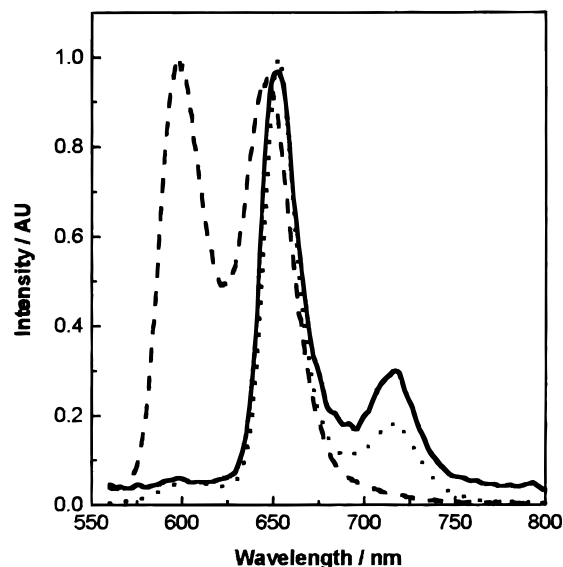


**Figure 3.** Corrected Fluorescence emission spectrum of: **P** (—), **P<sub>Zn</sub>** (---), and **P<sub>Zn</sub>-P** dyad (•••) in DCM,  $\lambda_{\text{ex}} = 550$  nm. The spectra have been normalized to one.

**TABLE 1: Photoelectrochemical Properties of Dyes**

dye	$E_{\text{ox}}^a$	$E_{\text{red}}^a$	$SE^b$	$E_{\text{ox}}^{*c}$	$\Delta E^d$	IPCE % <sup>e</sup>	LHE %	$\Phi_{\text{inj}}\eta_c$
P	0.97	-1.18	1.90	-0.93	0.73	32 (24)	92	0.34
P <sub>Zn</sub>	0.82		2.09	-1.27	1.07	6 (4)	55	0.11
P <sub>Zn</sub> -P			1.90			11 (8)	87	0.12
P <sub>Zn</sub> -ester	0.79	-1.27	2.09					
P-amide	0.91	-1.19	1.90					

<sup>a</sup> Ground-state oxidation and reduction potential (V vs SCE). <sup>b</sup> First excited singlet state (eV). <sup>c</sup> Oxidation potential of excited dyes (V vs SCE). <sup>d</sup> Driving force for photoinduced electron transfer  $\Delta E = -e(E_{\text{ox}}^* - E_{\text{FB}})$  (eV). <sup>e</sup> Maximum IPCE at Soret bands under bias voltage = 0.1 V. In parentheses values without bias.

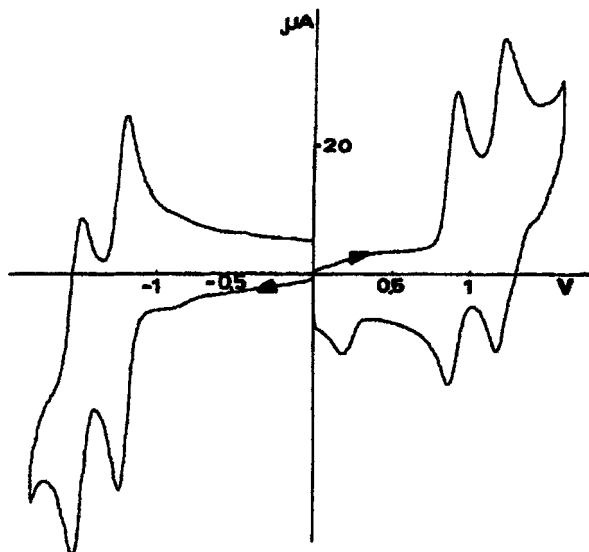


**Figure 4.** Cyclic voltammogram at a platinum electrode ( $A = 0.25$  cm<sup>2</sup>) of **P-amide** 0.48 mM in DCE containing 0.1 M TBAHFP as supporting electrolyte. Sweep rate = 0.100 V/s.

fluorescence excitation spectra are essentially identical in the 500–700 nm range. This indicates that singlet–singlet energy transfer is nearly complete.<sup>38</sup> Thus, no matter which porphyrin moiety is excited in the **P<sub>Zn</sub>-P** dyad, always the excited singlet state of **P** is formed. These results are in complete agreement with those obtained for other structurally related porphyrins,

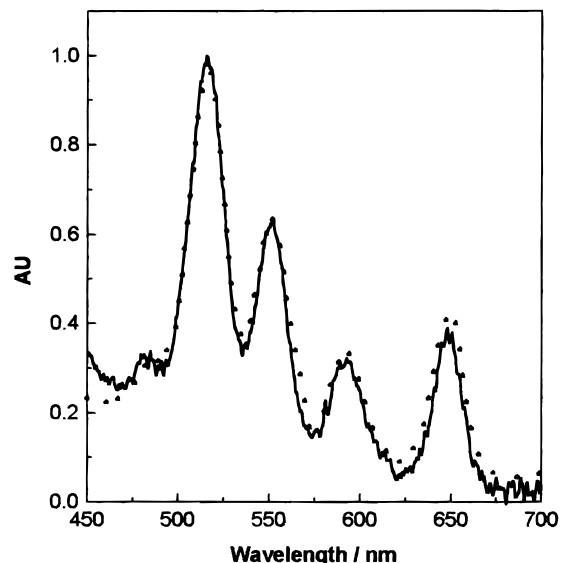
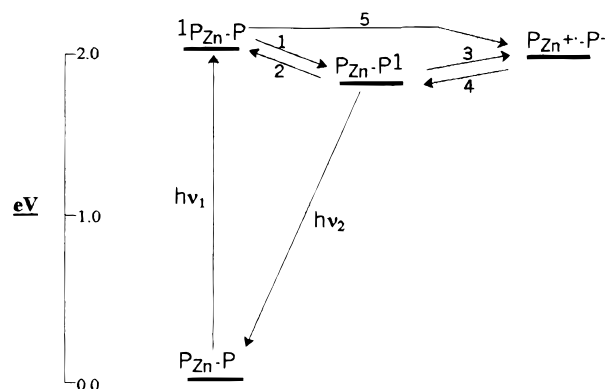


**Figure 5.** Corrected fluorescence excitation (—) and absorption (•••) spectra of **P<sub>Zn</sub>-P** in DCM solution. The emission was measured at 717 nm. Both spectra were normalized at 515 nm.

**SCHEME 1**



where quantitative singlet–singlet energy transfer was observed.<sup>38,52</sup>

**Properties of the ITO/SnO<sub>2</sub>/Dye Electrodes. Absorption and Emission Spectra.** Porphyrin adsorption onto the semiconductor produces strong violet–green coloration of the film. The electrodes have absorbance values between 0.6 and 1 at the absorption maximum (Soret band). Thus, the porosity of the film allows high harvesting of the dye molecules onto the semiconductor surface. The amount of the dyes adsorbed was determined by soaking the dye-loaded electrodes in a known volume of DCM for at least 2 h, after which the UV–visible absorption spectrum of the resulting solution was obtained. For ITO/SnO<sub>2</sub>/P, an average surface loading of  $\approx 4 \times 10^{-9}$  mol cm<sup>-2</sup> was obtained.

The electronic spectra of the studied compounds on the ITO/SnO<sub>2</sub>/dye electrode and in DCM solution are shown in Figure 2. In the adsorbed films, the Soret and Q-bands show electronic transitions similar to those observed for monomeric absorption in DCM. However, on the electrodes the bands are broader and shifted in comparison with those in solution. This may be caused by the interaction of the porphyrins with the polar surface of the electrode, as well as the possible formation of porphyrin aggregates due to its high concentration onto the electrode.

The emission spectrum of an ITO/SnO<sub>2</sub>/P<sub>Zn</sub>-P electrode also resembles that of the **P** porphyrin, with no significant emission

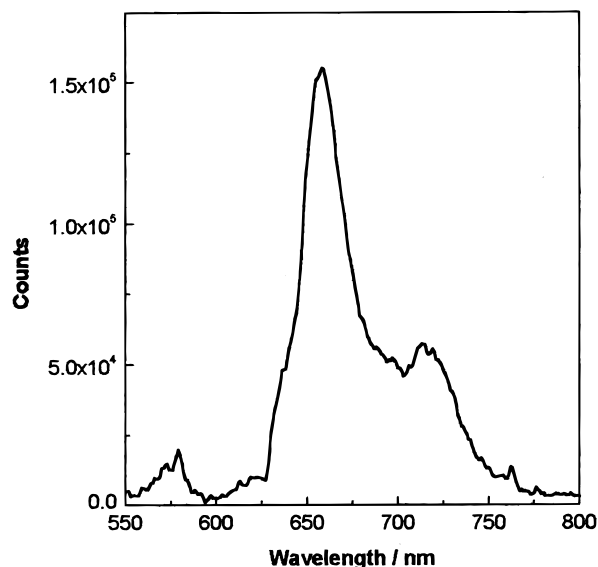


**Figure 6.** Corrected fluorescence emission spectrum of ITO/SnO<sub>2</sub>/P<sub>Zn</sub>-P.  $\lambda_{\text{ex}} = 550$  nm.

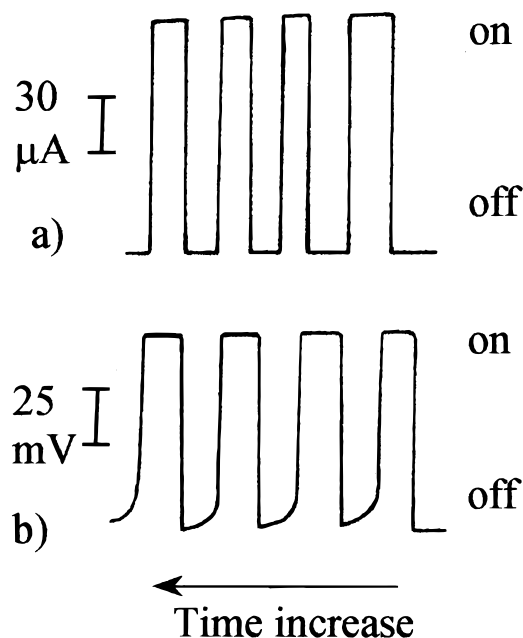


**Figure 7.** On-off illumination cycles of (a) photocurrent and (b) photovoltage at an ITO/SnO<sub>2</sub>/P electrode. Excitation wavelength  $\lambda = 425$  nm,  $I_{\text{inc}} = 1.55$  mW cm<sup>-2</sup> (photocurrent was obtained at 0.2 anodic bias vs Ag/AgCl).

from the P<sub>Zn</sub> moiety at the excitation wavelength of 550 nm (Figure 6). This result suggests that singlet-singlet energy transfer from the P<sub>Zn</sub> to P occurs also when the dye is in adsorbed state.

**Photoelectrochemistry.** The ITO/SnO<sub>2</sub>/dye electrodes are photoelectrochemically active. Anodic photocurrents and photopotentials are observed upon excitation of these electrodes with visible light, indicating that the electrons flow from the illuminated electrode to the ITO contact. A typical result for ITO/SnO<sub>2</sub>/P electrode is shown in Figure 7. The photocurrent is reproducible under repeated on-off illumination cycles and decays by ~15% over 2 h during continuous operation of the cell. 1,4-Benzoquinone, formed by oxidation of H<sub>2</sub>Q in water, has been reported to convert photochemically to 2-hydroxy-1,4-benzoquinone, which in turn polymerizes to give a brownish-black polymer.<sup>53</sup> The decreased photocurrents observed with

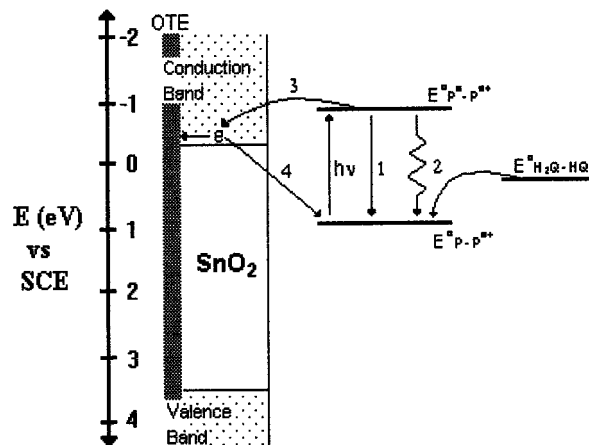


**Figure 8.** Energy level diagram for the spectral sensitization of ITO/SnO<sub>2</sub>/P electrode.

aqueous hydroquinone are thus consistent with the formation of a light-filtering polymer that slowly coats the electrode surface, producing a continuous drop in photocurrent.

A photovoltage of ~0.12 V was achieved following the excitation of an ITO/SnO<sub>2</sub>/P electrode ( $\lambda_{\text{ex}} = 420$  nm, incident intensity = 1.55 mW cm<sup>-2</sup>), as is shown in Figure 7b. The photovoltage observed in the absence of dye was negligible. This confirmed that the photovoltage generation was entirely initiated by the excitation of the dye.

Figure 8 shows a schematic illustration of a possible mechanism for the generation of anodic photocurrent in an ITO/SnO<sub>2</sub>/P electrode in contact with aqueous H<sub>2</sub>Q. After production of the excited state by photon absorption ( $h\nu$ ), several pathways are possible: (1) radiative relaxation, (2) thermal (nonradiative) relaxation, or (3) interfacial charge injection. When the latter occurs, the injected electron hops from particle to particle until it ultimately reaches the ITO layer, producing observable photocurrent. Although, the efficiency for charge injection is adversely influenced by charge recombination (4) at the dye-film interface, it can be partially suppressed in the presence of the sacrificial reductant (in this case H<sub>2</sub>Q).

**Effect of the H<sub>2</sub>Q Concentration.** The variation of the concentration of the sacrificial donor (H<sub>2</sub>Q) present in the electrolyte affects the efficiency of photocurrent generation, as shown in Figure 9 for an ITO/SnO<sub>2</sub>/P electrode. The photocurrent is maxima at H<sub>2</sub>Q = 0.01 M. When H<sub>2</sub>Q is absent, the anodic photocurrent is small and a cathodic current is observed when the light is turned off, as the oxidized sensitizer retraps photoinjected electrons. In the presence of H<sub>2</sub>Q, a higher stationary anodic photocurrent is observed during illumination and the cathodic current is suppressed. This observation is in agreement with other dye-sensitized oxide electrodes.<sup>17</sup> Similar results were obtained with the P<sub>Zn</sub> and P<sub>Zn</sub>-P dyad.

**Dependence of the Photocurrent on the Applied Potential.** The effect of an applied potential on the observed photocurrent generation is shown in Figure 10 for an ITO/SnO<sub>2</sub>/P electrode. The observed photocurrent increases with anodic bias in every case, which could be due to the increase in the collection efficiency of the injected electrons. It has been reported that the application of an external electrical bias to a dye-sensitized nanocrystalline TiO<sub>2</sub> film can result in a rapid acceleration of the rate of charge recombination process, while the electron injection kinetics are rather insensitive to it.<sup>54-56</sup> When the excited sensitizer injects electrons into the SnO<sub>2</sub> particle, the trapped electrons hop through the film to the ITO conducting

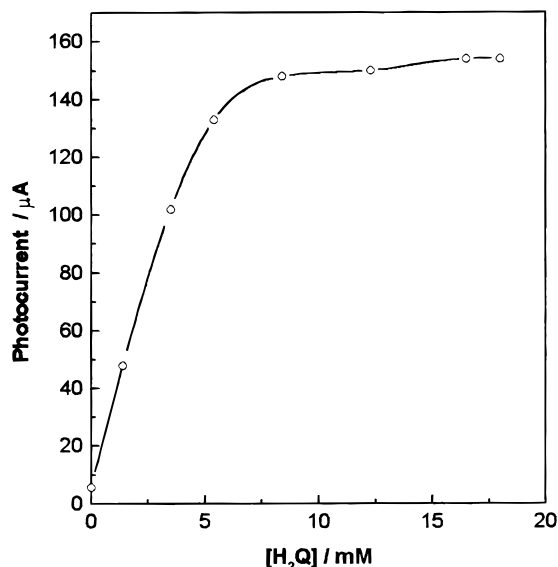


**Figure 9.** Photocurrent of an ITO/SnO<sub>2</sub>/P electrode as function of the H<sub>2</sub>Q concentration. All the other conditions for photocurrents measurements were the same as in Figure 7.

surface being the driving force the electric field produced by the applied bias. With a cathodic bias, charge recombination competes with charge injection.<sup>13,34</sup> Upon illumination of the electrodes under cathodic bias (i.e., < -200 mV), a decay of anodic photocurrent and a growth of cathodic current upon termination of illumination could be observed. The growth of cathodic current arises from a back electron transfer from reduced SnO<sub>2</sub> nanoparticles to the photooxidized adsorbed dye.<sup>57</sup>

**Photocurrent Action Spectra.** The action spectrum (measured under 0.1 V positive bias) closely matches the absorption spectrum of ITO/SnO<sub>2</sub>/dye in all cases, see Figure 11. The incident-photon-to-photocurrent efficiencies (IPCE) were evaluated from eq 1.<sup>27,32,58</sup>

$$\text{IPCE (\%)} = 100 (i_{\text{sc}}/1240)/(I_{\text{inc}} \lambda) \quad (1)$$

where  $i_{\text{sc}}$  is the short circuit photocurrent (A cm<sup>-2</sup>),  $I_{\text{inc}}$  is the incident light intensity (W cm<sup>-2</sup>), and  $\lambda$  is the excitation wavelength (nm). The close correspondence between the photocurrent action spectrum and the absorption spectrum of the electrodes confirms that photosensitization has successfully extended the photocurrent response of the electrodes into the visible region.

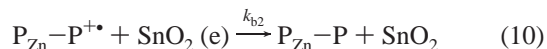
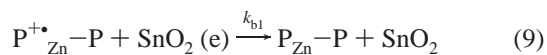
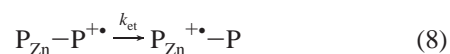
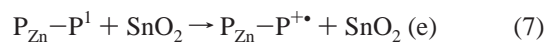
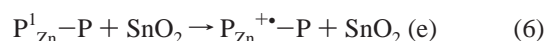
Maximum IPCE of ~6%, 32%, and 11% were obtained at the Soret band of ITO/SnO<sub>2</sub>/P<sub>Zn</sub>, ITO/SnO<sub>2</sub>/P, and ITO/SnO<sub>2</sub>/P<sub>Zn</sub>-P, respectively, by using [H<sub>2</sub>Q] = 0.01 M and bias voltage = 0.1 V. There are several reasons for this difference, and they may be linked to the factors that determine IPCE, namely, the light harvesting efficiency (LHE) of the dye, the charge injection yield ( $\Phi_{\text{inj}}$ ) from the excited dye to the semiconductor, and the charge collection efficiency,  $\eta_{\text{c}}$ , of the system. The IPCE in terms of these parameters can be written<sup>27,35</sup> as:

$$\text{IPCE \%} = \text{LHE (\%)} \Phi_{\text{inj}} \eta_{\text{c}} \quad (2)$$

Table 1 summarizes the results of IPCE, LHE, and the product  $\Phi_{\text{inj}}\eta_{\text{c}}$  for the three dyes at the Soret band. As it can be observed, P<sub>Zn</sub> gives lower photocurrent efficiency than the unmetallized porphyrin, despite that the driving force for charge injection is higher in the metallized one. For a dye adsorbed on a semiconductor the driving force for photoinduced electron

transfer from the dye to the semiconductor is the energy gap, defined as  $\Delta E = -e(E_{\text{ox}}^* - E_{\text{FB}})$ ,<sup>59</sup> where  $E_{\text{ox}}^*$  is the oxidation potential of the excited dye (estimate subtracting the excitation energy from the redox potentials of the molecule in the ground state<sup>24,25</sup>),  $E_{\text{FB}}$  is the flat band potential of the semiconductor ( $\sim -0.2$  V vs SCE),<sup>32</sup> and  $e$  is the electronic charge. The  $E_{\text{ox}}$  and  $E_{\text{ox}}^*$  potentials are shown in Table 1 for the monomers that are present in the P<sub>Zn</sub>-P dyad. The more negative  $E_{\text{ox}}^*$  value for the metallized porphyrin should facilitate the electron transfer from the excited state of the dye to the semiconductor. As it has been observed, free-base tetracarboxyphenyl porphyrin exhibit 5- to 8-fold slower charge recombination kinetics than the analogue Zn metallized porphyrin, when they are used in the spectral sensitization of TiO<sub>2</sub> nanostructured electrodes.<sup>55,56</sup>

On the other hand, the product  $\Phi_{\text{inj}}\eta_{\text{c}}$  in the P<sub>Zn</sub>-P molecule is very similar to that of the P<sub>Zn</sub>. Thus, a possible reason for the low photocurrent efficiency in the dyad is the contribution of P<sub>Zn</sub> moiety to the back electron-transfer process.<sup>55,56</sup> In the case of other SnO<sub>2</sub>/chlorophyll<sup>13,14</sup> and SnO<sub>2</sub>/Zn-porphyrin<sup>17</sup> electrodes, the back electron-transfer process showed to be the major limiting factor in achieving high IPCE values, producing low efficiency of photon-to-photocurrent conversion.<sup>13,34,60</sup> Consequently, it is proposed that in the dyad molecule the oxidized state of the P<sub>Zn</sub> moiety acts as fast electron acceptor in the back electron transfer. The complete mechanism is summarized in eqs 3–10



Both porphyrin moieties in dyad can be excited by light absorption (eqs 3 and 4), but the lack of fluorescence from the metallized unit (both in solution and in adsorbed state) indicates that energy transfer (eq 5) can compete with the electron transfer process to the semiconductor (eq 6). Thus, it is probable that most of the photocurrent is generated from the excited state of the free base moiety (eq 7). The heterogeneous electron transfers (eqs 6 and 7) indicate the formation of two different radical cations, (P<sup>+</sup><sub>Zn</sub>-P and P<sub>Zn</sub>-P<sup>+</sup>), but the electron-transfer process from the zinc porphyrin to the oxidized free base (eq 8) is an exergonic process, as it is inferred from the 0.12 V difference in the oxidation potentials (estimated from the first oxidation potential of P<sub>Zn</sub>-ester and P-amide, Table 1). Hence, it is proposed that the presence of the oxidized metallized porphyrin enhances the back electron-transfer process<sup>55,56</sup> (eq 9), producing lower photocurrent yields in the dyad molecule than in P. Moreover, the photocurrent generation efficiency for the

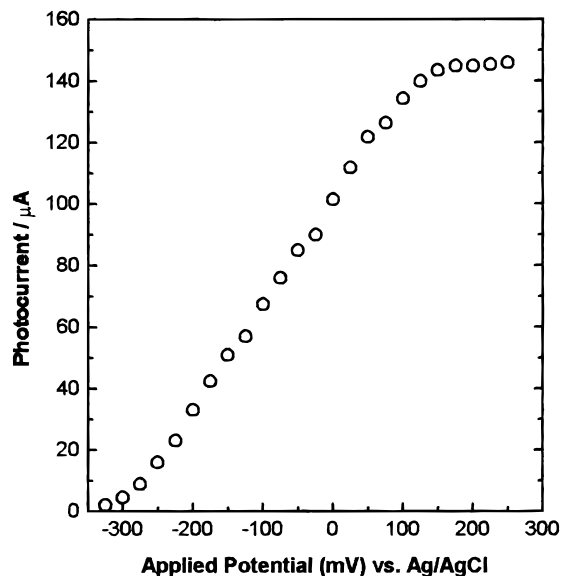


**Figure 10.** Dependence of incident photon-to-current efficiency IPCE (%) on applied bias for ITO/SnO<sub>2</sub>/P. Electrode was excited at absorption maximum of the dye, 425 nm.

ITO/SnO<sub>2</sub>/P<sub>Zn</sub>-P electrode, taken at the Q-band where only the free base moiety absorbs (i.e., 650 nm), is always around three times lower than in the ITO/SnO<sub>2</sub>/P electrode. If there were no effects of the presence of P<sub>Zn</sub> moiety in the dyad, both photocurrents should be near the same. On the other hand, an effect resulting from the orientation of the dyad over the SnO<sub>2</sub> surface (i.e., whether it is the P moiety or the P<sub>Zn</sub> moiety that gets attached to SnO<sub>2</sub> surface) might also play a role in determining the IPCE of the dyad, and cannot be rejected.

#### 4. Conclusions

The phophrin dyad molecule and its moieties have been used in the spectral sensitization of wide band gap semiconductor colloidal particles. The SnO<sub>2</sub> film modified with porphyrin dyes exhibits photoresponse in the visible region. The close match between the photocurrent action spectrum and the absorption spectrum shows that the photosensitization mechanism is operative in extending the photocurrent response of ITO/SnO<sub>2</sub>/dye electrode to the visible.

Nearly complete singlet-singlet energy transfer from the P<sub>Zn</sub> to P has been observed in the P<sub>Zn</sub>-P dyad, even when the dye is in the adsorbed state. Moreover, the photocurrent efficiency in the dyad and P<sub>Zn</sub> are lower than the P moiety, although the  $E_{ox}^*$  value is more negative for the metallized porphyrin, which should facilitate the electron transfer from the excited state of the dye to the semiconductor. Consequently P<sub>Zn</sub> is less efficient than P in the heterogeneous charge-transfer process, but is a suitable energy donor, acting as "antenna" in the dyad molecule. The fact that in the generation of photoelectrical effects the dyad is less effective in comparison with P is explained considering that the metallized porphyrin enhances the back electron-transfer process, producing low photocurrent yield.

**Note Added in Proof.** When this manuscript was in the publication process, a work was published by Koehorst, R. B. M.; Boschloo, G. K.; Savenije, T. J.; Goossens, A.; Schaafsma, T. J. *J. Phys. Chem. B* **2000**, 104, 2371. This paper deals with the spectral sensitization of TiO<sub>2</sub> substrates by porphyrin heterodimers. Monolayers of these dimers enhance the spectral response of the semiconductor with respect to the monomeric sensitizer by intramolecular energy transfer.

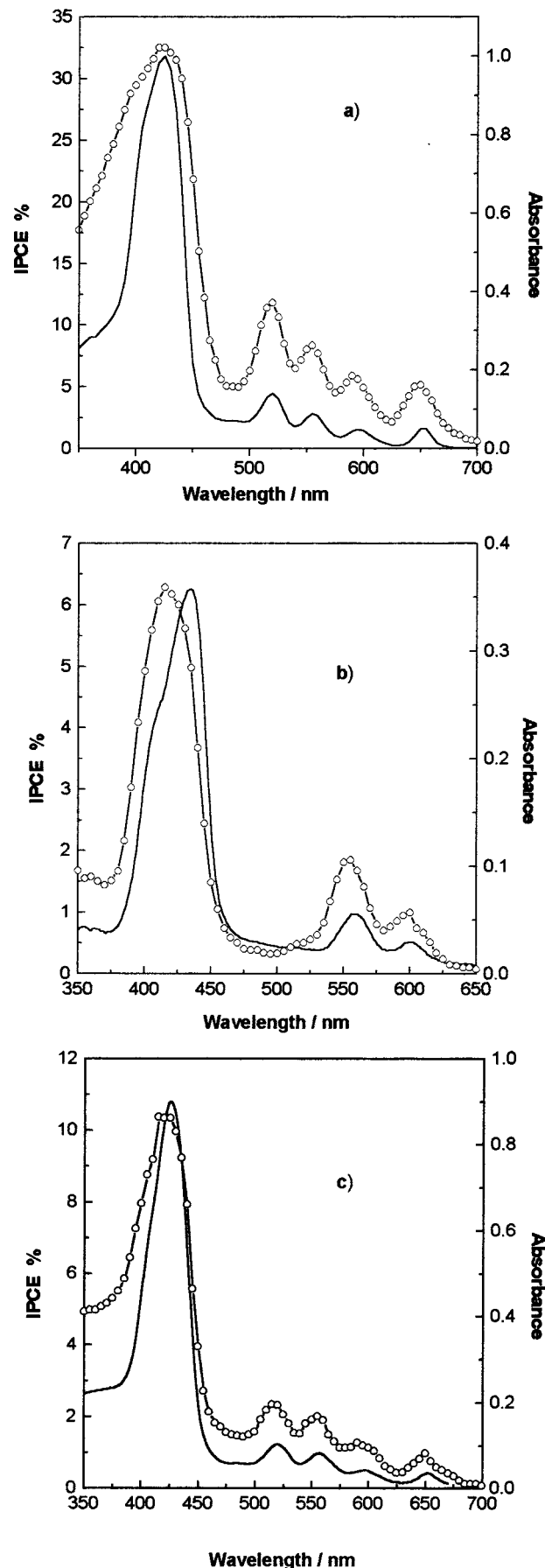


**Figure 11.** Absorption spectra (—) and photocurrent action spectra, IPCE (○) of ITO/SnO<sub>2</sub>/dye electrodes modified with (a) P, (b) P<sub>Zn</sub>, and (c) P<sub>Zn</sub>-P dyad. All other conditions for photocurrent measurements were the same as in Figure 7.

**Acknowledgment.** We are grateful to Consejo Nacional de Investigaciones Científicas y Técnicas (CONICET-Argentina); Agencia Nacional de Promoción Científica y Tecnológica (FONCYT-Argentina); Consejo Provincial de Investigaciones Científicas y Técnicas (CONICOR-Córdoba) and Secretaría de Ciencia y Técnica de la Universidad Nacional de Río Cuarto (SECYT-UNRC) for financial support. F.F. thanks CONICET for a research fellowship.

## References and Notes

- (1) Feher, G.; Allen, J. P.; Okamura M. I.; Rees, D. C. *Nature* (London) **1989**, *339*, 111.
- (2) Gust, D.; Moore, T. *Top. Curr. Chem.* **1991**, *159*, 103.
- (3) Gust, D.; Moore, T. *Adv. Photochem.* **1991**, *16*, 1.
- (4) Wasielewski, M. R. *Chem. Rev.* **1992**, *92*, 435.
- (5) Steinberg-Yfrach, G.; Rigaud, J.; Durantini, E. N.; Moore, A. L.; Gust, D.; Moore, T. A. *Nature* **1998**, *392*, 479.
- (6) Land, E. J.; Lexa, D.; Bensasson, R. V.; Gust, D.; Moore, T. A.; Moore, A. L.; Liddell, P. A.; Nemeth, G. A. *J. Phys. Chem.* **1987**, *91*, 4831.
- (7) Peychal-Heiling, G.; Wilson, G. S. *Anal. Chem.* **1971**, *43*, 545.
- (8) Gregg, B.; Fox, M. A.; Bard, A. J. *J. Phys. Chem.* **1990**, *94*, 1586.
- (9) Fox, M. A.; Pan, H. L.; Jones, W.; Melamed, D. *J. Phys. Chem.* **1995**, *99*, 11523.
- (10) Kay, A.; Grätzel, M. *J. Phys. Chem.* **1993**, *97*, 6272.
- (11) Kay, A.; Humphry-Baker, R.; Grätzel, M. *J. Phys. Chem.* **1994**, *98*, 952.
- (12) Hotchandani, S.; Kamat, P. V. *Chem. Phys. Lett.* **1992**, *191*, 320.
- (13) Bedja, I.; Hotchandani, S.; Carpentier, R.; Fessenden, R.; Kamat, P. V. *J. Appl. Phys.* **1994**, *75*, 5444.
- (14) Bedja, I.; Kamat, P. V.; Hotchandani, S. *J. Appl. Phys.* **1996**, *80*, 4637.
- (15) Deng, H.; Mao, H.; Lu, Z.; Li, J.; Xu, H. *J. Photochem. Photobiol. A: Chem.* **1997**, *110*, 47.
- (16) Boschloo, G. K.; Goossens, A. *J. Phys. Chem.* **1996**, *100*, 19489.
- (17) Otero, L.; Osora, H.; Li, W.; Fox, M. A. *J. Porphyrins Phthalocyanines* **1998**, *2*, 123.
- (18) Deng, H. H.; Lu, Z. H. *Supramol. Sci.* **1998**, *5*, 669.
- (19) Wienke, J.; Schaafsma, T. J.; Goossens, A. *J. Phys. Chem. B* **1999**, *103*, 2702.
- (20) Sclottwein, D.; Jaeger, N.; Wöhrle, D. *Ber. Bunsen-Ges., Phys. Chem.* **1991**, *95*, 1526.
- (21) Fermin, D. J.; Ding, Z. F.; Duong, H. D.; Brevet, P. F.; Girault, H. H. *J. Phys. Chem. B* **1998**, *102*, 10334.
- (22) Shimizu, Y.; Higashiyama, T.; Fuchita, T. *Thin Solid Films* **1998**, *331*, 279.
- (23) Takahashi K.; Goda T.; Yamaguchi T.; Komura T.; Murata K. *J. Phys. Chem. B* **1999**, *103*, 4868.
- (24) Memming, R. *Comprehensive Treatise of Electrochemistry*; Plenum Press: New York, 1983; Chapter 7, p 529.
- (25) Gerischer, H.; Willig, F. *Top. Curr. Chem.* **1976**, *61*, 31.
- (26) O'Regan, B.; Grätzel, M. *Nature (London)* **1991**, *353*, 737.
- (27) Nazeeruddin, M. K.; Kay, A.; Rodicio, I.; Humphry-Baker, R.; Muller, E.; Liska, P.; Vlachopoulos, N.; Grätzel, M. *J. Am. Chem. Soc.* **1993**, *115*, 6382.
- (28) Smestad, G. *Sol. Energy Mater. Sol. Cells* **1994**, *32*, 273.
- (29) Moser, J. E.; Bonhôte, P.; Walder, L.; Grätzel, M. *Chimia* **1997**, *51*, 28.
- (30) Hagfeld, A.; Grätzel, M. *Chem. Rev.* **1995**, *95*, 49.
- (31) Kamat, P. V. *Prog. React. Kinet.* **1994**, *19*, 277.
- (32) Bedja, I.; Hotchandani, S.; Kamat, P. V. *J. Phys. Chem.* **1994**, *98*, 4133.
- (33) Kamat, P. V. *CHEMTECH* **1995**, *25*, 22.
- (34) Kamat, P. V.; Bedja, I.; Hotchandani, S.; Patterson, L. *J. Phys. Chem.* **1996**, *100*, 4900.
- (35) Bedja, I.; Kamat, P. V.; Hua, X.; Lappin, A. G.; Hotchandani, S. *Lagmuir* **1997**, *13*, 2398.
- (36) Sugihara, H.; Singh, L. P.; Sayama, K.; Arakawa, H.; Nazeeruddin, M. K.; Grätzel M. *Chem. Lett.* **1998**, *10*, 1005.
- (37) Burnside, S. D.; Brooks, K.; McEvoy, A. J.; Grätzel, M. *Chimia* **1998**, *52*, 557.
- (38) Gust, D.; Moore, T.; Moore, A.; Gao, F.; Luttrull, D.; DeGraziano, J.; Ma, X.; Makings, L.; Lee, S.-J.; Trier, T.; Bittersmann, E.; Seely, G.; Woodward, S.; Bensasson, R.; Rougée, M.; De Schryver F.; Van der Auweraer, M. *J. Am. Chem. Soc.* **1991**, *113*, 3638.
- (39) Rodriguez, J.; Kirmaier, C.; Johnson, M. R.; Friesner, R. A.; Holten D.; Sessler, J. L. *J. Am. Chem. Soc.* **1991**, *113*, 1652.
- (40) Gust, D.; Moore, T. A.; Moore, A. L.; Leggett, L.; Lin, S.; DeGraziano, J.; Hermant, R. M.; Nicodem, D.; Craig, P.; Seely, G.; Nieman, R. A. *J. Phys. Chem.* **1993**, *97*, 7926.
- (41) Gust, D.; Moore, T. A.; Moore, A. L.; Kang, H. K.; DeGraziano, J. M.; Liddell, P. A.; Seely, G. R. *J. Phys. Chem.* **1993**, *97*, 13637.
- (42) Ravikumar, M.; Pandian, R. P.; Chandrashekar, T. K. *J. Porphyrin Phthalocyanines* **1999**, *3*, 70.
- (43) Tsuchiya, S. *J. Am. Chem. Soc.* **1999**, *121*, 48.
- (44) Bignozzi, C.; Argazzi, R.; Indelli, M.; Scandola, F. *Sol. Energy Mater. Sol. Cells* **1994**, *32*, 229.
- (45) Lee C-H.; Lindsey, J. S. *Tetrahedron* **1994**, *50*, 11427.
- (46) Durantini, E. N.; Silber, J. J. *Synth. Commun.* **1999**, *29*, 3353.
- (47) Fungo, F.; Otero, L.; Sereno, L.; Silber, J. J.; Durantini, E. N. *J. Mater. Chem.* **2000**, *10*, 645.
- (48) Gust, D.; Moore, T. A.; Moore, A. L.; Devadoss, C.; Lindell, P. A.; Hermant, R.; Nieman, R. A.; Demanche, L. D.; DeGraziano, J. M.; Gouni, I. *J. Am. Chem. Soc.* **1992**, *114*, 3590.
- (49) Gust, D.; Moore, T. A.; Bensasson, R. V.; Mathis, P.; Land, E. J.; Chachaty, C.; Moore, A. L.; Liddell, P. A.; Nemeth, G. A. *J. Am. Chem. Soc.* **1985**, *107*, 3631.
- (50) Anton, J. A.; Loach, P. A. *J. Heterocycl. Chem.* **1975**, *12*, 573.
- (51) Kadish, K. M.; Guo, N.; Van Caemelbecke, E.; Paolesse, R.; Monti, D.; Tagliatesta, P. *J. Porphyrin Phthalocyanines* **1998**, *2*, 439.
- (52) Gust, D.; Moore, T. A.; Moore, A.; Lee, S.-J.; Bittersmann, E.; Luttrull, D.; Rehms, A.; DeGraziano, J. M.; Ma, X.; Gao, F.; Belford, R.; Trier, T. *Science* **1990**, *248*, 199.
- (53) Dabestani, R.; Bard, A. J.; Campion, A.; Fox, M. A.; Mallouk, T.; Webber, T.; White, J. M. *J. Phys. Chem.* **1988**, *92*, 1872.
- (54) Haque, S. A.; Tachibana, Y.; Klug, D. R.; Durrant, J. R. *J. Phys. Chem. B* **1998**, *102*, 1745.
- (55) Haque, S. A.; Tachibana, Y.; Willis, R. L.; Moser, J. E.; Grätzel, M.; Klug, D. R.; Durrant, J. R. *J. Phys. Chem. B* **2000**, *104*, 538.
- (56) Tachibana, Y.; Haque, S. A.; Mercer, I. P.; Durrant, J. R.; Klug, D. R. *J. Phys. Chem. B* **2000**, *104*, 1198.
- (57) Li, W.; Osora H.; Otero L.; Duncan, D. C.; Fox, M. A. *J. Phys. Chem.* **1998**, *102*, 5333.
- (58) Vlachopoulos, P.; Liska, P.; Augustynski, J.; Grätzel, M. *J. Am. Chem. Soc.* **1988**, *110*, 1216.
- (59) Hasshimoto, K.; Hiramoto, M.; Lever, A. B. P.; Sakata, T. *J. Phys. Chem.* **1988**, *92*, 1016.
- (60) Nasr, C.; Kamat, P.V.; Hotchandani, S. *J. Phys. Chem. B* **1998**, *102*, 10047.